A model for Textile Reinforced Concrete under imposed uniaxial deformations

Jens Hartig* **and Ulrich Häußler-Combe***
Institute of Concrete Structures, Technische Universität Dresden
01062 Dresden, Germany
e-mail: jens.hartig@tu-dresden.de, ulrich.haeussler-combe@tu-dresden.de

Abstract

This paper presents investigations regarding the uniaxial load-bearing behaviour of the novel cement-based composite Textile Reinforced Concrete under restrained imposed deformations. Imposed deformations might result from shrinkage and hydration heat of the cementitious matrix and external temperature changes. As a consequence, bond degradation between matrix and reinforcement as well as matrix cracks can occur, which can impair both the load-bearing capacity as well as serviceability. For modelling, a one-dimensional finite element model is applied consisting of bar elements representing the load-bearing behaviour of either matrix or reinforcement and bond elements to model the interaction in between. Imposed deformations are applied as additional strains to the bar elements. The model provides results regarding the global load-bearing response of the composite, which can be directly compared with experimental results. Additionally, information regarding local stress distributions are available, which can be usually not determined in experiments. Thus, further insight in the load-bearing behaviour of the composite is obtained with the model.

Keywords: composites, concrete, cracks, finite element methods, numerical analysis, textiles

1. Introduction

Textile Reinforced Concrete (TRC) is a composite of a fine-grained concrete matrix and a reinforcement of multi-filament yarns processed to textile structures, see e. g. Refs. [4] and [8]. The reinforcement material can be chosen according to the desired application of the composite. For structural applications, fibres exhibiting sufficiently large Young's modulus and high tensile strength such as alkali-resistant (AR) glass or carbon fibres are usually applied. Moreover, these fibre materials do not suffer from corrosion when embedded in the alkaline matrix, see Refs. [5, 6, 7], which allows for a considerable reduction of concrete cover compared to conventional reinforced concrete and the design of thin structural elements, see Fig. 1.

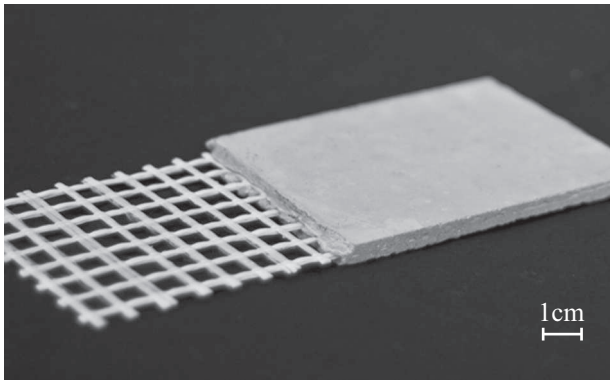

Figure 1: Textile reinforced concrete; photo from Ref. [11]

A special load case is imposed deformation, which might be critical for the integrity of structural elements of TRC if restrained. Imposed deformations might be caused by external sources, e. g. external temperature changes, and due to the application of a cement-based matrix by internal sources, e. g. hydration heat and shrinkage. The effect of hydration heat can be assessed as small as the thickness of TRC structural elements is usually small (in the range of a few centimetres) and, thus, thermal gradients are small as well.

Restrained imposed deformations might result in deterioration of the composite at least for two reasons. On the one hand, it might lead to additional cracking of the matrix if the stabilised cracking state is not already reached due to previous loading. On the other hand, the bond between matrix and reinforcement might be degraded. This can be especially critical in the case of thermal loading if matrix and reinforcement have different thermal expansion coefficients. Carbon fibres are known to exhibit negative thermal expansion in axial direction at room temperature while the matrix has positive thermal expansion. To investigate the influence of imposed deformations on the uniaxial load-bearing behaviour of TRC, the model presented in Ref. [11, 12, 13] is enhanced by imposed strains.

In the subsequent section, the material behaviour of the constituents of TRC, the matrix and the reinforcement, as well as the composite itself is described briefly. Afterwards, the model for the simulation of the load-bearing behaviour of TRC is presented. This is followed by computational results regarding the response of the composite to restrained imposed deformations. At the end, the findings are summarised and some conclusions are drawn.

2. Selected material properties

2.1. Fine-grained concrete

The matrix used for the composite under consideration is a fine-grained concrete with a maximum aggregate size of 1 mm and a CEM III cement as binder, see e. g. Refs. [5] and [14]. It is known that due to a relatively slow hydration speed characteristic of CEM III cements also low hydration heat per time is produced, see e. g. Ref. [20]. Additionally structural elements of TRC are usually thin and, thus, only small temperature gradients

*The authors gratefully acknowledge the financial support of this research from Deutsche Forschungsgemeinschaft DFG (German Research Foundation) within the Sonderforschungsbereich (Collaborative Research Center) 528 "Textile Reinforcement for Structural Strengthening and Retrofitting" at Technische Universität Dresden.

occur. Thus, the effect of hydration heat of the matrix is negligible for TRC. Nevertheless, external temperature reduction will lead to contraction of the matrix, which can result also in concrete cracks if restrained. The thermal expansion coefficient of cementitious matrices is $\alpha_{T,m} \approx 1.0 \cdot 10^{-5}\,\mathrm{K}^{-1}$.

A further material property of the matrix, which results in imposed deformations is shrinkage. As the matrix shows relatively large shrinkage, matrix cracks are supposed to occur if the shrinkage strains are restrained. The maximum shrinkage strains of the fine-grained concrete consisting of autogenous and drying shrinkage can be estimated with 0.2 %, which is an order of magnitude larger than the ultimate tensile strain.

Under uniaxial tensile loading, the material behaviour of cementitious matrices can be assumed linear elastic up to a tensile strength f_{mt}. According to Ref. [14], Young's modulus and tensile strength of the fine-grained concrete have values of $E_{m0} \approx 28{,}500\,\mathrm{N/mm^2}$ and $f_{mt} \approx 5\,\mathrm{N/mm^2}$. After exceeding f_{mt}, brittle failure can be assumed in a first approach. Experiments reveal, however, a certain post-cracking resistance also referred to as tension softening, which depends on several properties of the matrix. It is, e. g., known that concretes with large rough aggregates show stronger post-cracking resistance than concretes with small round aggregates, see e. g. Refs. [16] and [20]. As the used fine-grained concrete has small round aggregates, relatively small post-cracking resistance can be expected. Tension softening of the applied fine-grained concrete was, hitherto, not experimentally investigated. Investigations on a similar matrix presented in Ref. [3] revealed, however, a fracture energy $G_f \approx 40\,\mathrm{N/mm}$ and crack width at complete crack face separation of $w_c \approx 0.2\,\mathrm{mm}$

2.2. Reinforcement

The fibres typically used for TRC are AR glass and carbon fibres. While AR glass has a positive thermal expansion coefficient of $\alpha_{T,g} \approx 5 \cdot 10^{-6}\,\mathrm{K}^{-1}$ similar to the matrix, carbon has a negative value of $\alpha_{T,c} \approx -1... - 5 \cdot 10^{-7}\,\mathrm{K}^{-1}$ in fibre direction at room temperature, see Refs. [9, 17]. Shrinkage is not observed for both fibre materials.

The uniaxial tensile behaviour of both reinforcement materials can be assumed as linear elastic up to failure reaching the tensile strength. The reinforcement yarns show usually a certain waviness resulting from the production process. The waviness leads to a delayed activation of the reinforcement and to larger deformations of the cracked composite compared to stretched fibres. The Young's modulus of the carbon fibres is with approximately $210{,}000\,\mathrm{N/mm^2}$ considerably higher than the value of glass fibres with approximately $80{,}000\,\mathrm{N/mm^2}$, see Ref. [1]. Moreover, the exploitable tensile strength is usually larger for the carbon fibres ($1000\text{-}2500\,\mathrm{N/mm^2}$) than for the glass fibres ($500\text{-}1500\,\mathrm{N/mm^2}$).

2.3. Composite

In the case of thermal loading, in TRC with AR glass reinforcement an almost compatible deformation of matrix and reinforcement is possible because the thermal expansion coefficients are similar. Thus, bond deterioration due to thermal loading shall be small. In contrast, the negative thermal expansion coefficient of carbon fibres might lead to considerable bond deterioration due to opposed deformations. Moreover, also matrix cracking might be increased in case of temperature reduction. In the case of matrix shrinkage, the reinforcement might restrain matrix deformations.

In general, the interface is stronger between AR glass fibres and concrete than between carbon fibres and concrete. However, for both cases bond can be considerably improved with additional coating, see e. g. Refs. [18, 19]. Moreover, different bond zones usually exist over the cross section of a yarn due to incomplete penetration with either matrix or coating, see e. g. Ref. [14]. Especially without additional coating the differences of the transferable bond stresses over the yarn cross section are large. In general, only the filaments in the so-called fill-in zone or sleeve zone, which is the outer layer of the yarn where matrix or coating intrudes continuously, are bonded initially by adhesion to the matrix. The adhesive bond is limited by the bond strength. When the bond strength is exceeded, bond degradation occurs, which is associated with a successive transition to frictional load transfer. For the load transfer in the core of the yarns where a negligible amount of matrix or coating material is present, frictional load transfer between the filaments is usually assumed.

2.4. Uniaxial load-bearing behaviour

The load-bearing behaviour of TRC due to tensile loading is usually determined with plate-shaped specimens. However, experimental results under imposed deformations are, hitherto, missing. An extensive experimental work on the tensile behaviour of TRC was carried out by Jesse [14]. Selected results are summarised in the following.

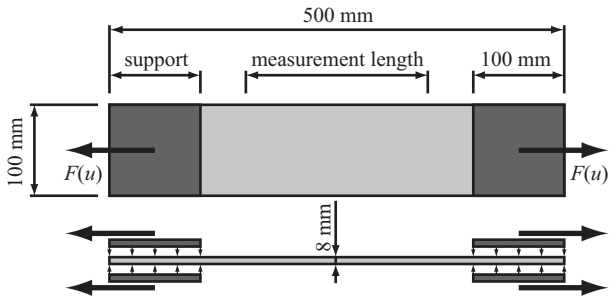

Figure 2: Test setup used by Jesse [14] for the determination of the tensile behaviour of TRC

The specimens, see Fig. 2, are usually applied with reinforcement ratios in a range of 1 % up to 3 %, which preserves multiple cracking of the matrix. The specimens are attached to testing machine by means of clamps. Loading is applied with displacement (u) control. During loading, forces F are measured with a load cell and relative displacements with extensometers on the surface of the specimen over a measurement length of 0.2 m. The forces are divided by the cross-sectional area of the specimen leading to a mean stress. The relative displacements are related to the measurement length resulting in a mean strain.

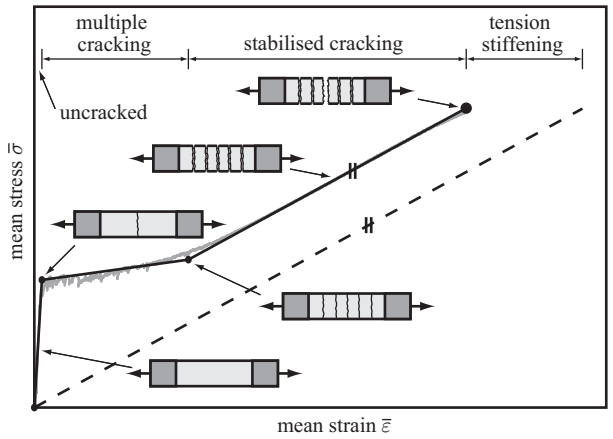

Figure 3: Typical mean stress-strain behaviour of TRC under uniaxial tensile loading; from [11]

A respective mean stress-strain relation under uniaxial tensile loading is shown in Fig. 3. It consists of three distinct state. The

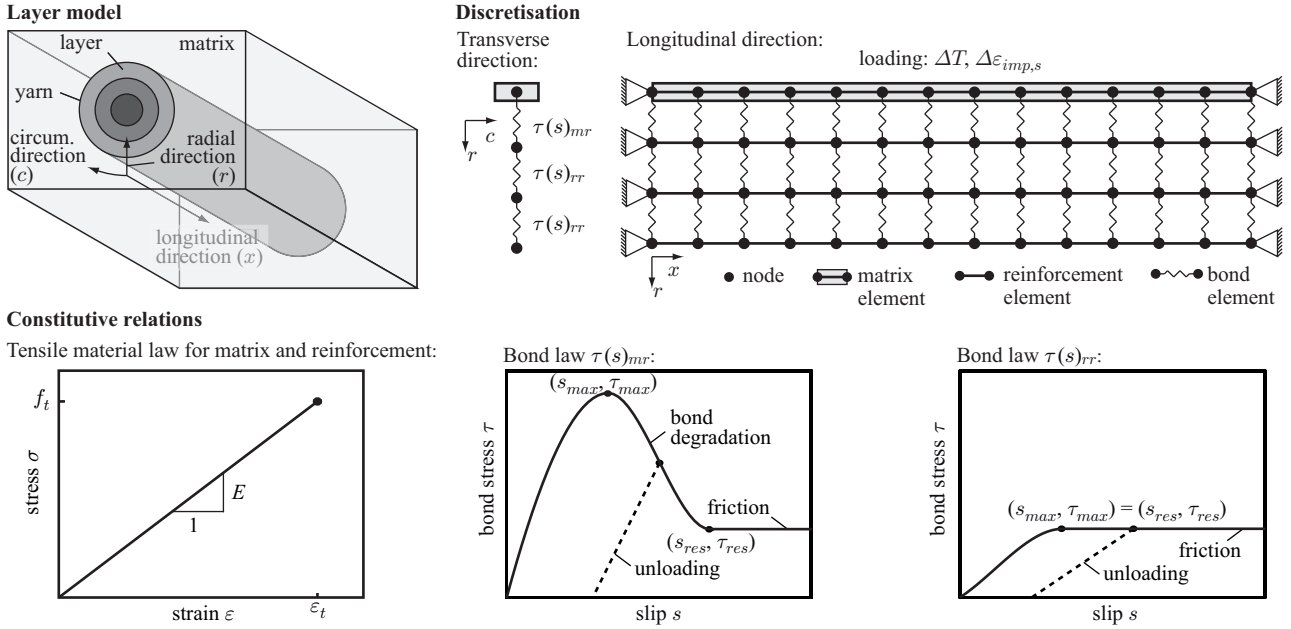

Figure 4: Layer model and constitutive relations

uncracked state were the matrix bears most of the load. When the tensile strength of the matrix is exceeded, the first matrix crack occurs and the mean stress drops. The reinforcement is activated and bridges the crack. Distant to the crack the load is transferred back to the matrix by means of bond mechanisms, which can be e. g. adhesion and friction. If a sufficient amount of reinforcement is available and the bond is sufficiently strong, the load can be further increased. This leads also to further matrix cracks. At a certain stage, crack spacing becomes too small to reach the matrix tensile strength again, which is also associated with bond degradation. At this stage, the state of multiple cracking is finished and the stabilised cracking state starts. The stabilised cracking state is primarily controlled by the material properties of the reinforcement and, thus, the slope of this state corresponds approximately to the stiffness of the plain reinforcement. However, also the matrix participates in load-bearing between the cracks leading to tension stiffening, i. e. reduced strains, compared to the stiffness corresponding to the reinforcement.

For imposed loading, such a mean stress-strain relation cannot be established because the mean strain is always approximately zero. Therefor, it might be advantageous to establish some mean stress-imposed strain relations. Nevertheless, similar load-bearing mechanisms as in the case of force-controlled loading involving, e. g., matrix cracking and bond degradation will appear.

3. Model

3.1. Geometrical characteristics

A model according to Refs. [11, 12, 13] based on the finite element method is applied, which consists of two types of elements. The model is shown schematically in Fig. 4. One-dimensional bar elements represent the uniaxial load-bearing behaviour of matrix and reinforcement or parts of it. In longitudinal direction x, which is also the loading direction, a sufficient number of bar elements are arranged in series to represent the interaction between the constituents of the composite as well as multiple cracking of the matrix appropriately. The matrix is modelled with one bar element chain assuming that shear gradients are small in the matrix due to small specimen thickness and small distances between reinforcing yarns. Furthermore, transverse deformations due to Poisson's ratio are neglected. For the reinforcement, it is assumed that all yarns behave approximately the same, which allows for representation of the entire system of a multitude of yarns by just one yarn embedded in matrix. As the reinforcement consists of a large number of single fibres, which are coupled discontinuously by matrix or coating cross-linkages, the yarn cross section needs to be modelled with more than one bar element chain. Therefore, a layer model, see Fig. 4, is applied assuming that only in radial direction r of the yarns differences in the load-bearing characteristics occur while they are negligible in circumferential direction c. The layer model provides also the cross-sectional areas A, which are property of the bar elements. The bar element chains are coupled at corresponding nodes with zero-thickness bond elements according to the scheme shown in Fig. 4. The bond surface areas S are also determined based on the layer model. Detailed descriptions of the determination of the values of A and S according to the layer model are given in Refs. [11, 13]. Boundary conditions are given with prescribed displacements at the end nodes of the bar element chains. Loading can be applied as prescribed displacements, forces and imposed strains.

3.2. Bar elements

The uniaxial material behaviour of the matrix and the reinforcement is modelled with two node bar elements as already pointed out. The element stiffness matrix is given with

$$\mathbf{K}_{bar} = \frac{EA}{L_{el}} \begin{bmatrix} 1 & -1 \\ -1 & 1 \end{bmatrix} \tag{1}$$

where E is the Young's modulus of the material, A is the cross-sectional area and L_{el} is the bar element length.

For both, matrix and reinforcement linear-elastic material behaviour according to the initial Young's modulus E_0 with limited tensile strength f_t is assumed in a first approach

$$\sigma = \begin{cases} E_0(\varepsilon - \varepsilon_{imp}) & \text{for} \quad 0 \leq (\varepsilon - \varepsilon_{imp}) \leq \frac{f_t}{E_0} \\ 0 & \text{for} \quad (\varepsilon - \varepsilon_{imp}) > \frac{f_t}{E_0} \end{cases} \tag{2}$$

with stress σ, measurable strain ε and imposed strain ε_{imp}. If ε_{imp} results from temperature changes ΔT, the respective im-

posed strain is $\varepsilon_{imp,T} = \alpha_T \Delta T$ with the thermal expansion coefficients α_T of the materials given in Section 2. Imposed strains due to shrinkage $\varepsilon_{imp,s}$ are prescribed to the matrix elements only. The main portion of strains due to matrix shrinkage occur at the early age of the matrix where also the material parameters change considerably. Such time-dependent changes are not taken into account in these investigations and it is assumed in a simplifying manner that material parameters are constant over time.

Tension softening of the matrix can be taken into account as implemented in Refs. [11, 12] applying the stress-crack width relation by Remmel [16] and the crack band approach by Bažant & Oh [2] for regularisation. The respective stress-strain relation is given for $f_{mt}/E_{m0} < (\varepsilon - \varepsilon_{imp}) < f_{mt}/E_{m0} + w_c/L_{el}$ with:

$$\sigma = f_{mt1} \exp\left(- \left(\frac{L_{el}\left((\varepsilon - \varepsilon_{imp}) - \frac{f_{mt}}{E_{m0}} \right)}{w_1} \right)^c \right) + f_{mt2} \left(1 - \frac{L_{el}\left((\varepsilon - \varepsilon_{imp}) - \frac{f_{mt}}{E_{m0}} \right)}{w_c} \right). \quad (3)$$

Equation (3) contains a form parameter c, two parameters f_{mt1} and f_{mt2} associated with the tensile strength f_{mt} as well as two characteristic crack widths w_1 and w_c. For the determination of the parameters and the derivative of Eq. 3, see Ref. [11]. Unloading in the softening range is implemented based on the concept of damage mechanics, i. e. with reduced stiffness. The crack width w of a cracked element can be determined as

$$w = \left(\varepsilon - \varepsilon_{imp} - \frac{f_{ct}}{E_{m0}} \right) L_{el}. \quad (4)$$

assuming that one bar element does only represent one crack.

3.3. Bond elements

The interaction between the matrix and the reinforcement as well as between the reinforcement layers is modelled with zero-thickness bond-link elements. The element stiffness matrix of the bond-link elements is given with

$$\mathbf{K}_{bond} = GS \begin{bmatrix} 1 & -1 \\ -1 & 1 \end{bmatrix} \quad (5)$$

where $G = d\tau/ds$ is the bond modulus and S is the bond area.

The constitutive relations of the bond elements are bond stress-slip (τ-s) relations, see Ref. [13]. The slip s is the relative displacement of the two nodes of a bond element. The τ-s relations are defined by supporting points (s, τ). Between these supporting points, it is interpolated. Therfor, the so-called PCHIP approach by Fritsch & Carlson [10], which uses piecewise cubic Hermite polynomials for interpolation is applied. The PCHIP approach ensures that the interpolation functions do not locally overshoot the values of the supporting points. Moreover, the smooth transition at the supporting of the bond law reduces, at least, numerical problems during computations at these points. Based on the PCHIP approach also the tangential bond modulus G needed in Eq. (5) can be determined, see Ref. [11].

Due to the incomplete penetration of the reinforcement with matrix or coating, different bond zones have to be taken into account over the yarn cross section. Therefore, two different bond laws $\tau(s)_{mr}$ and $\tau(s)_{rr}$ are applied, see Fig. 4.

Bond law $\tau(s)_{mr}$ is applied between the matrix and the layer representing the filaments in the fill-in zone of the yarn. Based on the assumption of adhesive bond, τ increases initially with increasing slip s. After exceeding the bond strength τ_{max}, bond degradation with transition to friction is assumed. This is modelled with a decreasing course of the τ-s relation until a residual bond stress value τ_{res}. Unloading is modelled based on the concept of plasticity, i. e. with a linear unloading path different to the loading path and remaining deformations. For the filament-filament interaction between the core layers primarily frictional load transfer is assumed. This is modelled in bond law $\tau(s)_{rr}$ with a bond strength τ_{max} equal to the frictional bond stress τ_{res}.

3.4. Numerical solutions

The cracking events in the matrix and the nonlinear bond laws lead to nonlinear systems of equations. Therefor, the load is applied incrementally and an iterative solution is performed. As solution method, the BFGS approach [15], which is a Quasi-Newton method, combined with line search is used. Matrix cracking events are limited to one per load step. When a crack occurred the system is recalculate on the same load step with a respectively modified stiffness matrix.

4. Simulations

4.1. Specification of the model

Exemplary simulations are carried out to show the abilities of the model. Unfortunately, a validation of the results cannot be performed, hitherto, as respective experimental data is not available. For the simulations, it is assumed that the specimens by Jesse [14] as shown in Fig. 2 are loaded with imposed deformations in the free part of the specimen on a length of 300 mm. The length of the bar elements is defined with 0.2 mm, which results in 1500 elements per bar element chain.

The concrete is modelled with one bar element chain, while the reinforcement is represented by five bar element chains according to the layer model described in Section 3.1. The outermost layer represents the filaments in the fill-in zone, which are connected adhesively to the matrix and are supposed to share their load uniformly or in other words globally. For the bond elements between the matrix and the outermost reinforcement bar element chain, bond law $\tau(s)_{mr}$ with values $\tau_{max} = 9\,\mathrm{N/mm^2}$, $s_{max} = 4{\cdot}10^{-3}$ mm, $\tau_{res} = 3\,\mathrm{N/mm^2}$ and $s_{res} = 8{\cdot}10^{-3}$ mm is applied. Due to the weak load transfer between the filaments in the core of the yarns resulting primarily from friction, local load-sharing depending on the radial position in the yarn has to be expected. Thus, the core of the yarn is finer discretised with four layers. Between the reinforcement bar element chains, bond elements with bond law $\tau(s)_{rr}$ and values $\tau_{max} = \tau_{res} = 3\,\mathrm{N/mm^2}$ and $s_{max} = \tau_{res} = 4{\cdot}10^{-3}$ mm is applied. The bond law parameters were estimated in a calibration process performed in Ref. [11].

The material properties of the matrix are applied as given in Section 2.1. Two types of simulations are carried out: neglecting and considering matrix tension softening. For the softening law Eq. (3), it is assumed that $c = 1$, $f_{mt1} = 4.9\,\mathrm{N/mm^2}$ and $f_{mt2} = 0.1\,\mathrm{N/mm^2}$. The cross-sectional area of the matrix is defined with $800\,\mathrm{mm^2}$ corresponding to Fig. 2. For the reinforcement, where the cases of glass and carbon reinforcement are taken into account, the material parameters are given in Section 2.2. For the carbon reinforcement, a thermal expansion coefficient of $\alpha_{T,c} = -5 \cdot 10^{-7}\,\mathrm{K^{-1}}$ is applied. However, reinforcement failure is not considered in the simulation. In a simplifying manner, it is assumed that the bond laws are identical for the glass-matrix interface and the carbon-matrix interface, which is not necessarily the case in reality as pointed out in Section 2.3. In the simulations, a reinforcement ratio of 2 % is applied. Glass and carbon yarns have usually different cross-sectional areas and, thus, bond-surface areas. In the following, values of two typical yarn types are used. For the glass reinforcement, the cross-sectional area of one yarn is assumed with $0.11\,\mathrm{mm^2}$ leading to 146 yarns. For the carbon reinforcement, a cross-sectional area of $0.45\,\mathrm{mm^2}$ is applied, which results in 36 yarns. For both yarn types, it is as-

sumed that 36 % of the cross-sectional correspond to filaments in the fill-in zone and 64 % to the yarn core. This ratio corresponds to a constant thickness of the layers in the layer model.

Two loading cases are investigated. The first case is matrix shrinkage where imposed strains of -0.1 % are applied incrementally decreasing to the matrix bar element chain. The second case is thermal loading where the temperature is reduced in the matrix and reinforcement elements incrementally to -100 K. For the matrix elements, this corresponds also to imposed strains of -0.1 %.

4.2. Results of the simulations

In this section, the results of the simulations are presented and analysed. At first, mean stress-imposed strain relations as shown in Figs. 5 and 6 are analysed. The mean stress is determined as the sum of the reaction forces at the nodes of one end of the model divided by the cross-sectional area of the matrix. The imposed strain is either the applied matrix shrinkage strain or the strain due to temperature reduction applied to matrix and reinforcement.

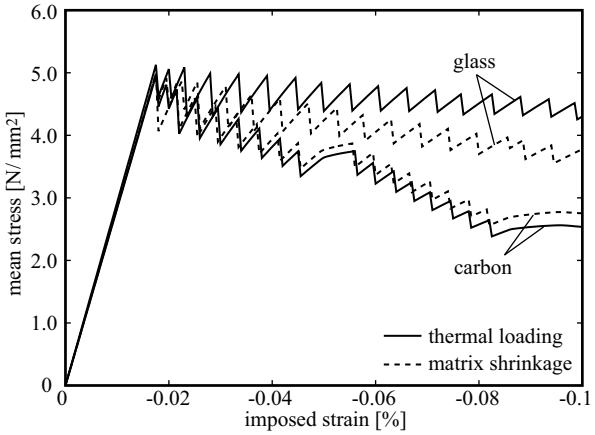

Figure 5: Mean stress-imposed strain relations neglecting matrix tension softening

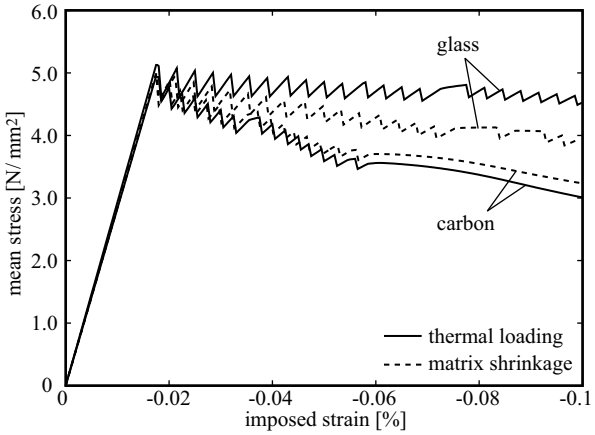

Figure 6: Mean stress-imposed strain relations considering matrix tension softening

It can be seen that the mean stress increases initially for all considered cases with increasing imposed strain until the tensile strength of the matrix is reached for the first time. Afterwards the mean stress drops until the reinforcement is activated to bridge the crack. As a sufficient amount of reinforcement and bond is available, the mean stress increases again until the next matrix crack occurs. However, the maximum mean stress levels decrease with increasing imposed strains, which can be explained with bond degradation resulting in a reduction of tension stiffening. The lower limit is given in the case of completely destroyed bond where only the imposed reinforcement deformations are restrained.

The smallest reduction is observable for the case of thermal loading and glass reinforcement, which result from contraction of the reinforcement compensating the loss of tension stiffening. This compensation does not occur in case of matrix shrinkage, which leads to a larger reduction of the mean stress. Even larger is this effect in the case of carbon reinforcement where the reinforcement expands with increasing temperature reduction. This is also the reason why the decrease of the mean stress is larger in the case of thermal loading than for matrix shrinkage. Matrix tension softening reduces the decrease of mean stress as a certain portion of normal stress is transferred in the matrix over the crack, see Fig. 6. However this effect decreases with increasing imposed strains because crack width increases and the stresses transferred in the matrix decrease.

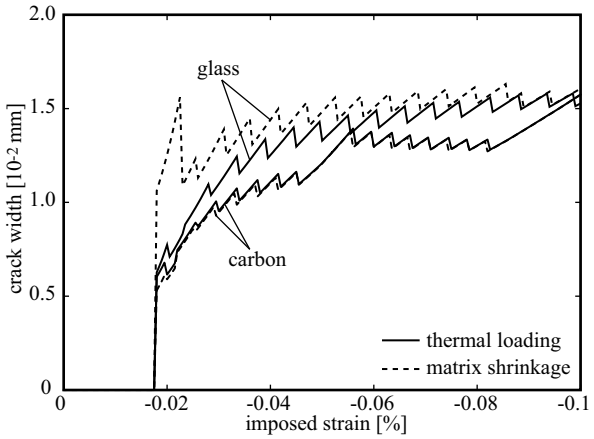

Figure 7: Mean crack width-imposed strain relations neglecting matrix tension softening

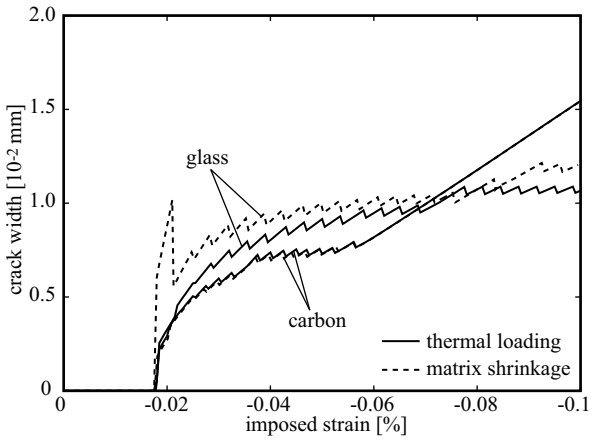

Figure 8: Mean crack width-imposed strain relations considering matrix tension softening

Figures 7 and 8 show the mean crack widths as a function of the imposed strains for the different reinforcement and loading cases neglecting and considering matrix tension softening. It can be seen that the mean crack widths increase with increasing imposed strains. The type of loading, i. e. matrix shrinkage or

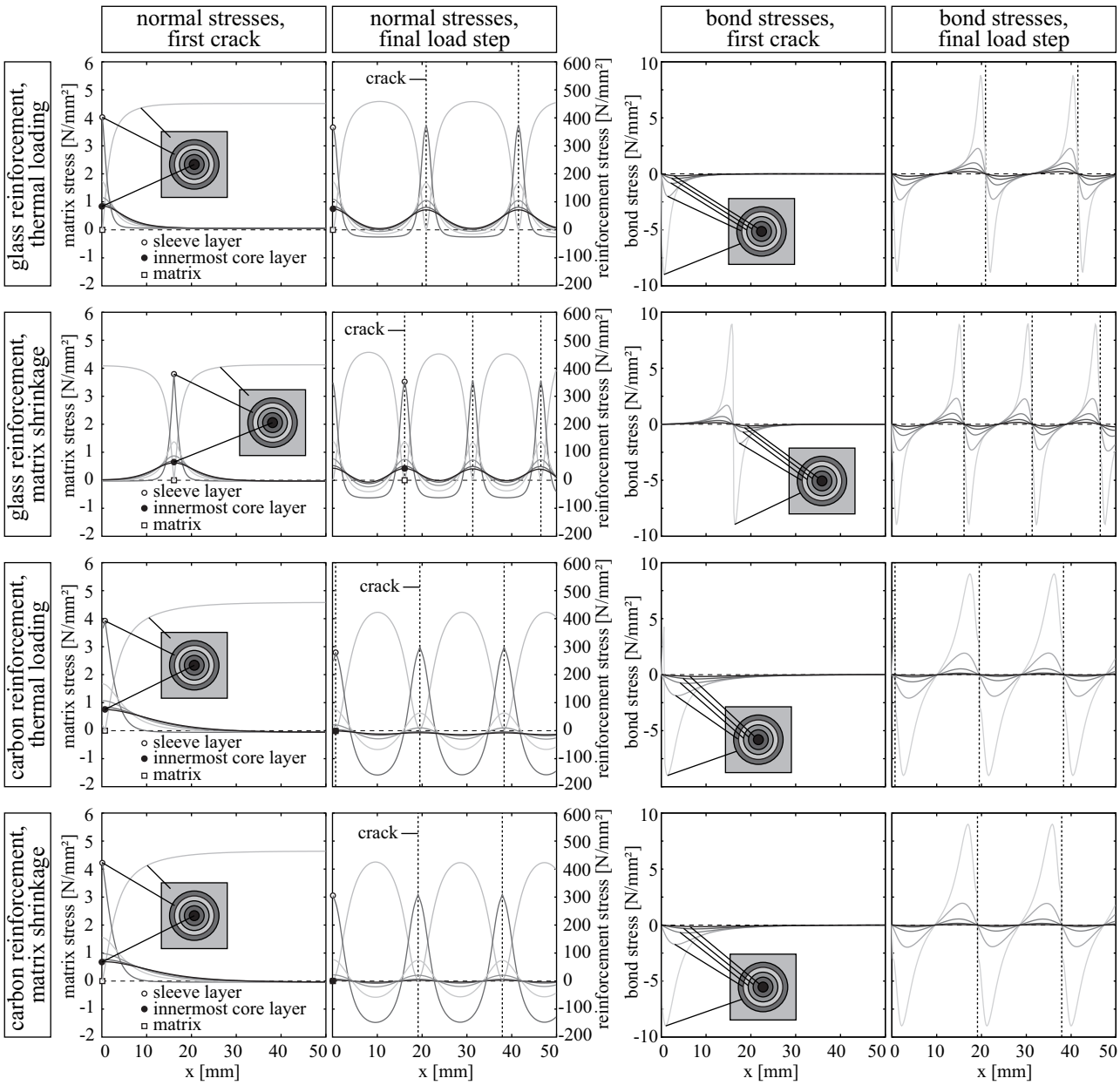

Figure 9: Normal and bond stress distribution on a range of $0 \leq x \leq 0.05\,\mathrm{m}$ neglecting matrix tension softening

thermal loading has minor influence on the crack width. The initial crack widths are smaller for carbon reinforcement because of the higher stiffness compared to the glass reinforcement, which restrains crack opening. Due to the larger bond surface area more cracks develop with glass reinforcement, which results in the effect that the stabilised cracking state is not reached during the range of loading. In contrast, in the simulations with carbon reinforcement the stabilised cracking state is reached in all cases. In the stabilised cracking state, the cracks open strongly leading to increasing crack widths.

Matrix tension softening initially restrains crack opening, which leads to a reduction of crack widths. For carbon reinforcement this leads also to a shortening of the strain range where cracking occurs but the numbers of the cracks are not influenced. For glass reinforcement also the numbers of cracks increase considering matrix tension softening.

Most of the aforementioned properties of the load-bearing behaviour of the composite can be explained by bond stress and normal stress distributions. Respective diagrams are shown in Figs. 9 and 10 for the load step corresponding to the first crack and the final load step. In the two left columns, normal stress distributions in the matrix and the reinforcement layers on a range of $0 \leq x \leq 0.05\,m$ are shown for the state after the first matrix crack and at the final load step. In the right two columns the respective bond stresses are shown.

It can be seen that the stress transfer length are larger in case of carbon reinforcement compared to glass reinforcement. This can be explained by the higher stiffness of the carbon reinforcement compared to the glass reinforcement. In all cases, the reinforcement possesses compressive stresses between the cracks in the final load step. This results from matrix contraction. The largest compressive stresses are observable for carbon reinforcement where these compressive stresses are slightly larger in the case of thermal loading compared to matrix shrinkage due to ad-

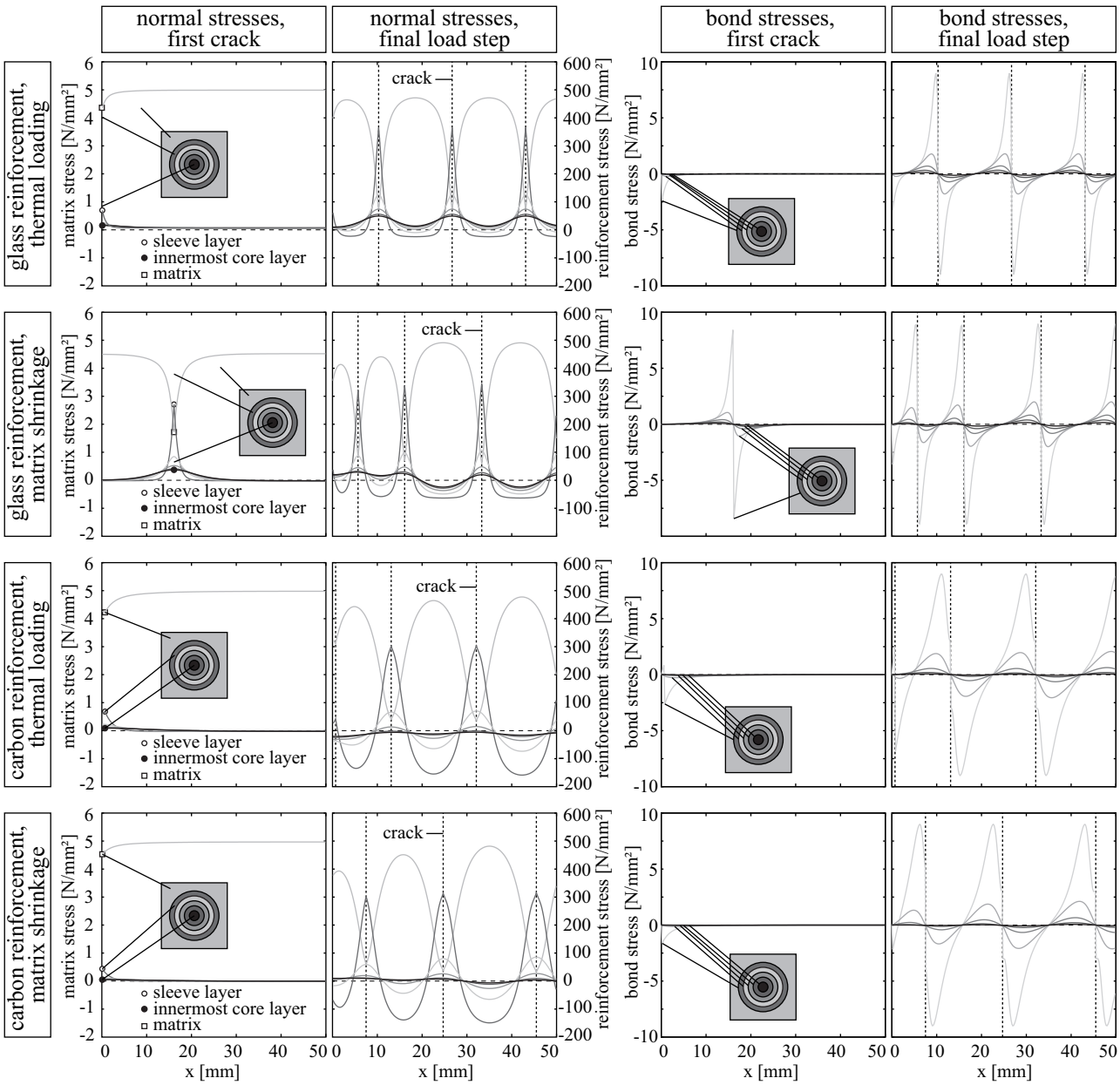

Figure 10: Normal and bond stress distribution on a range of $0 \leq x \leq 0.05$ m considering matrix tension softening

ditional compressive stresses because of the negative thermal expansion of carbon. In the case of glass reinforcement, the compressive stresses are smaller due to lower stiffness of the reinforcement. Moreover, the compressive stresses are further reduced in the case of thermal loading due to the contraction of the reinforcement, which is only slightly smaller than the contraction of the matrix according to the applied thermal expansion coefficients.

The normal stress distributions are directly associated with bond stress distributions. Bond stresses equal or close to zero indicate intact bond in case of monotonic loading without fibre pull-out phenomena. Intact bond is observable at the end of the stress transfer length (e.g. in the bond stress distributions for the case of the first crack) and in the centre between two cracks (e.g. in the bond stress distributions for the final load step). Degraded bond exists in the range between the crack position and the position where the bond stress reaches the bond strength. For glass reinforcement relatively large ranges of intact bond are observable. In contrast, the bond strength fronts have reached relatively large distances to the crack positions in the final load step for carbon reinforcement, which indicates strong bond degradation. Moreover, it can be seen that differences in the bond stress distribution between the case of matrix shrinkage and thermal loading are small for carbon reinforcement. Thus, the negative thermal expansion coefficient of carbon reinforcement seems to have a subordinate influence. The reason is that the deformations of the carbon reinforcement are more than one order of magnitude lower than those of the matrix.

In the case considering matrix tension softening, it can be seen that especially in the case of the first crack considerable normal stresses are transferred in the matrix, which results in reduced reinforcement and bond stresses. However, this effect reduces with increasing loading. Although in the final load step still stress is transferred over the matrix in the crack the normal stress dis-

tributions of the reinforcement and bond stresses differ not much from the cases neglecting matrix tension softening. Only in the case of glass reinforcement more cracks develop and, thus, crack spacing is decreased.

5. Summary and conclusions

In this paper, a numerical model within the framework of the Finite Element Method for the simulation of the uniaxial tensile load-bearing behaviour of Textile Reinforced Concrete exposed to imposed deformations was presented and results of exemplary simulations were shown. Despite a relatively simple geometrical representation of the composite, the model gains complexity by nonlinear formulations of the constitutive relations, such as limited tensile strength resulting in matrix cracks, matrix tension softening and nonlinear bond laws.

The simulations covered the simulation of the load-bearing behaviour of tensile bars exposed to matrix shrinkage and thermal loading applied as imposed deformations. The deformations were restrained by fixation of the bar ends. The presented results of the model are stress-imposed strain relations, crack width-imposed strain relations and stress distributions between matrix and reinforcement. It was shown that due to the imposed strains matrix cracking occurred, which also led to bond degradation. The most detrimental effect on bond was observed in the case of carbon reinforcement. However, the bond degradation resulted primarily from the high stiffness of the reinforcement. The negative thermal expansion coefficient of the carbon fibres, which leads to an expansion of the reinforcement while the matrix contracts, has due to its low absolute value compared to the matrix a subordinate influence on the load-bearing behaviour. Accordingly, it is of secondary interest whether the imposed deformation results from matrix shrinkage or thermal loading. In contrast, matrix shrinkage has in case of glass reinforcement a more detrimental effect than thermal loading where the contraction of the reinforcement leads to more compatible deformations of matrix and reinforcement.

In summary, restrained imposed deformations lead to a stiffness reduction of the composite due to matrix cracking and to degradation of bond. In the considered range of imposed loading, the reinforcement stresses were considerably below characteristic tensile strength values. Nevertheless, for additional external loading less load-bearing reserves remain. Even though stress gradients might be reduced due to creep of the matrix, the reduced composite stiffness and the degraded bond remains. Bond degradation might also necessitate the increase of the anchorage length of the reinforcement.

References

[1] Abdkader, A., *Charakterisierung und Modellierung der Eigenschaften von AR-Glasfilamentgarnen für die Betonbewehrung*, Dissertation, Technische Universität Dresden, Dresden, 2004.

[2] Bažant, Z.P. and Oh, B.H., Crack band theory for fracture of concrete, *Mater. Struct.*, 16, pp. 155-177, 1983.

[3] Brockmann, T., *Mechanical and fracture mechanical properties of fine grained concrete for textile reinforced composites*, Dissertation, RWTH Aachen, Aachen, 2005.

[4] Brameshuber, W. (Ed.), *State-of-the-Art Report of RILEM Technical Committee 201 TRC: Textile Reinforced Concrete (RILEM Report 36)*, RILEM Publications S.A.R.L., Bagneux, 2006.

[5] Butler, M., *Zur Dauerhaftigkeit von Verbundwerkstoffen aus zementgebundenen Matrices und alkaliresistenten Glasfaser-Multifilamentgarnen*, Dissertation, Technische Universität Dresden, Dresden, 2009.

[6] Butler, M., Mechtcherine, V. and Hempel, S., Experimental investigations on the durability of fibre-matrix interfaces in textile-reinforced concrete, *Cem. Concr. Compos.*, 31, pp. 221-231, 2009.

[7] Butler, M., Mechtcherine, V. and Hempel, S., Durability of textile reinforced concrete made with AR glass fibre: effect of the matrix composition, *Mater. Struct.*, 43, pp. 1351-1368, 2010.

[8] Curbach, M. and Jesse, F. (Eds.), *Textilbeton - Theorie und Praxis: Proceedings of the 4. Kolloquium zu textilbewehrten Tragwerken (CTRS4) und zur 1. Anwendertagung*, Technische Universität Dresden, Dresden, 2009.

[9] Ehlig, D., Jesse, F. and Curbach, M., Textilbeton verstärkte Platten unter Brandbelastung, *Beton- und Stahlbetonbau*, 105, pp. 102-110, 2010.

[10] Fritsch, F.N. and Carlson, R.E., Monotone Piecewise Cubic Interpolation, *SIAM J. Numer. Anal.*, 17, pp. 238-246, 1980.

[11] Hartig, J.U., *Numerical investigations on the uniaxial tensile behaviour of Textile Reinforced Concrete*, Dissertation, Technische Universität Dresden, Dresden, 2011.

[12] Hartig, J. and Häußler-Combe, U., A model for Textile Reinforced Concrete exposed to uniaxial tensile loading, *Proceedings of 18th International Conference in Computer Methods in Mechanics (CMM 2009)*, Kuczma, M., Wilmański, K., Szajna, W. (Eds.), The University of Zielona Góra Press, Zielona Góra, pp. 203-204, 2009.

[13] Hartig, J., Häußler-Combe, U. and Schicktanz, K., Influence of bond properties on the tensile behaviour of Textile Reinforced Concrete, *Cem. Concr. Compos.*, 30, pp. 898-906, 2008.

[14] Jesse, F., *Tragverhalten von Filamentgarnen in zementgebundener Matrix*, Dissertation, Technische Universität Dresden, Dresden, 2004.

[15] Matthies, H. and Strang, G., The solution of non-linear finite element equations, *Int. J. Numer. Methods Eng.*, 14, pp. 1613-1626, 1979.

[16] Remmel, G., *Zum Zug- und Schubtragverhalten von Bauteilen aus hochfestem Beton*, *DAfStb Heft* 444, Beuth, Berlin, 1994.

[17] Sauder, C., Lamon, J. and Pailler, R., Thermomechanical properties of carbon fibres at high temperatures (up to 2000 °C), *Compos. Sci. Technol.*, 62, pp. 499-504, 2002.

[18] Scheffler, C., Gao, S.L., Plonka, R., Mäder, E., Hempel, S., Butler, M. and Mechtcherine, V., Interphase modification of alkali-resistant glass fibres and carbon fibres for textile reinforced concrete I: Fibre properties and durability, *Compos. Sci. Technol.*, 69, pp. 531-538, 2009.

[19] Scheffler, C., Gao, S.L., Plonka, R., Mäder, E., Hempel, S., Butler, M. and Mechtcherine, V., Interphase modification of alkali-resistant glass fibres and carbon fibres for textile reinforced concrete II: Water adsorption and composite interphases, *Compos. Sci. Technol.*, 69, pp. 905-912, 2009.

[20] van Mier, J.G.M., *Fracture processes of concrete: assessment of material parameters for fracture models*, CRC Press, Boca Raton, 1996.